International Journal of Technology
http://ijtech.eng.ui.ac.id

Research Article

Experimental and Numerical Assessment of Heat-Affected Zone Fracture Toughness in Flux-Cored Arc Welded AISI 1015 Steel

Pavel Michel Almaguer Zaldívar[1], Alexis Cordovés García[2*], José Alejandro Martínez Grave de Peralta[3], Jesús Rodríguez Flores[2], Ricardo Lorenzo Ávila Rondón[4]

[1]Computer-Aided Design and Manufacturing Studies Center (CE-CAD/CAM), Faculty of Engineering, Holguín University, Holguín 80100, Cuba

[2]Engineering Systems Research and Consulting Group (GICSI), Faculty of Engineering Sciences and Industries, Universidad UTE, Quito 170527, Ecuador

[3]Applied Mechanics Department, Faculty of Engineering, Holguín University, Holguín 80100, Cuba

[4]Unidad Laguna, Universidad Autónoma de Coahuila, Torreón 27087, México

[*]Corresponding author: alexis.cordoves@ute.edu.ec; Tel.: +593-2-299-0800

Abstract: Fracture toughness is a key parameter for assessing structural integrity in welded joints, particularly within the heat-affected zone (HAZ), where microstructural transformations induced by welding may reduce crack resistance. This study proposes and validates an integrated experimental–analytical–numerical methodology for estimating the HAZ fracture toughness in flux-cored arc-welded (FCAW) AISI 1015 steel using non-instrumented Charpy V-notch impact testing. A metallography-assisted computer-aided design protocol ensured accurate and traceable notch positioning within the HAZ before machining. Fracture toughness was estimated by establishing correlations between the impact absorbed energy and the critical stress intensity factor. An energy-based analytical formulation was derived to determine the equivalent dynamic load for finite element coupling, and uncertainty was evaluated using a combined statistical and instrumental contribution framework. The experimentally obtained fracture toughness was $K_{Ic} = 62.19 \pm 1.6$ MPa·m$^{1/2}$ ($k = 2$, ≈95% confidence level), while the numerical simulation yielded a value of approximately 77.94 MPa·m$^{1/2}$, showing reasonable agreement. An approximate 10% reduction relative to the base material confirms that the HAZ is the critical fracture-controlling region. The proposed framework provides a practical and reproducible alternative to conventional fracture mechanics testing.

Keywords: Charpy impact test; Fracture toughness; Heat-affected zone; Numerical simulation; Welded joints

1. Introduction

Welded joints' integrity is critical to structural safety because welding introduces microstructural heterogeneity, stress concentrators, and local property variations that govern crack initiation and propagation (Jovanovic et al., 2022). The resulting toughness depends on several factors, including weld geometry, filler composition, loading mode, local stress–strain fields, and residual stresses (Cao et al., 2020; Purnama et al., 2020; Shin et al., 2025).

Within this context, fracture mechanics tests quantify crack growth resistance using parameters such as crack tip opening displacement (CTOD) and plane strain fracture toughness (K_{Ic}), providing rigorous characterization (Lee et al., 2025). However, standardized procedures (ASTM E1820-20b) are complex and expensive (ASTM International, 2020). The Charpy V-notch impact test (ASTM E23/ISO 148-1) measures the total energy absorbed during predominantly Mode I impact (CVN) (ASTM International, 2002; Chaouadi, 2024; International Organization

https://doi.org/10.14716/ijtech.v17i4.8262
Received November 2025; Revised January 2026; Accepted April 2026

for Standardization (ISO), 2016). Although CVN is not a fracture mechanics parameter, empirical and semi-empirical CVN–K_{Ic} correlations enable indirect toughness estimation without fatigue pre-cracking or complex instrumentation (Afzali et al., 2024b; Yildiz, 2022). Despite the dynamic–quasi-static differences, the underlying deformation mechanisms support their complementary use (Chaouadi et al., 2025; de Sonis et al., 2023).

CVN–fracture toughness correlations exhibit material- and calibration-dependent variability (Yildiz, 2022). Consequently, several predictive approaches based on microstructural descriptors, strength parameters, and data-driven models have been proposed (Kumar et al., 2021; Li et al., 2024a; Pan & Song, 2024). Experimental–numerical validation of small-specimen methodologies integrating Charpy energy with crack-tip parameters has also been reported (Ajmal et al., 2023; El Alami et al., 2024; Peinado et al., 2024), while master curve methods further support Charpy-based toughness estimation (Chaouadi, 2024).

These challenges become more pronounced in welded joints, particularly within the heat-affected zone (HAZ), where thermal cycles induce microstructural transformations that often reduce toughness relative to the base and filler metals (Narowlansky et al., 2024; Pała & Wciślik, 2024; Viseras Pico et al., 2022). Coarse-grained subzones are especially vulnerable when post-weld heat treatment is not optimized (Lojen & Vuherer, 2020). Although experimental investigations have confirmed degraded HAZ performance (Li et al., 2024b), they frequently lack precise documentation of notch localization near the fusion line, which may compromise the local representativeness of CVN measurements (Afzali et al., 2024b; Jovanovic et al., 2022; Li & Iyama, 2024). Table 1 summarizes the most relevant findings from the specialized literature and establishes the conceptual framework linking previous studies with this work's objectives.

Table 1 Summary of Relevant Findings from the Literature

Author(s)	Focus	Relevance to Present Study
(Kumar et al., 2021)	CVN–K_{Ic} empirical correlation	Demonstrates feasibility of estimating K_{Ic} from Charpy energy
(Yildiz, 2022)	Dispersion in CVN–K_{Ic} correlations	Highlights need for material-specific calibration
(Viseras Pico et al., 2022)	HAZ toughness in HSLA steel	Shows HAZ sensitivity and limited notch-placement detail
(Jovanovic et al., 2022); (Afzali et al., 2024a)	HAZ fracture evaluation	Report HAZ toughness reduction without explicit CAD-based localization
(Cao et al., 2020)	FEM simulation of Charpy test	Supports numerical validation of impact behavior
(El Alami et al., 2024)	Experimental–numerical Charpy validation	Confirms agreement between simulated and measured impact energy
Tao et al. (2023)	Microstructure–toughness relationships	Yield strength and microstructure in HAZ toughness correlations

A significant gap remains in the evaluation of fracture toughness in low-carbon steels such as AISI 1015, particularly in FCAW welded joints. Existing studies mainly focus on microalloyed steels and conventional fracture mechanics tests without explicitly representing the dynamic impact behavior. No energy-based model linking Charpy impact energy to fracture toughness in the HAZ has been clearly established.

From a multidisciplinary engineering perspective, addressing this problem requires integrating metallography, computer-aided design-assisted geometric scaling, classical materials mechanics, fracture mechanics, and finite element simulation within a coherent energy-based framework. The following fundamental contributions are presented in this study.

Contributions of this work:

1. Metallography–CAD protocol for the traceable positioning of the Charpy notch within the HAZ before machining.

2. Energy-consistent analytical estimation of impact load, enabling coupling of non-instrumented Charpy tests with finite element method to estimate fracture parameters.

3. Experimental–numerical cross-validation of the HAZ of AISI 1015 steel welded by FCAW, including replication and mesh convergence verification.

The article is organized into five sections. First, we present a theoretical background on fracture toughness and Charpy–fracture mechanics correlations. The experimental and numerical methods, including the notch-location protocol, are described in the following section. Then, the dynamic load derivation based on energy conservation is introduced. Finally, the results are discussed and conclusions are drawn.

2. Methods

Welded joints were made by flux-cored arc welding (FCAW) on a Miller CP-302 welding machine, manufactured in Wisconsin, USA, using industrial-grade CO_2 shielding gas supplied by Praxair/Linde (USA). Welded specimens were fabricated from AISI 1015 low-carbon steel, produced by Aceros y Materiales Ferrosos AMF (Monterrey, Mexico), with a tensile strength (σ_u) between 345 and 430 MPa (normalized condition). The filler metal used was AWS A5.20 E71T-1 flux-cored tubular wire, supplied by Lincoln Electric (Cleveland, USA), with a cross-sectional diameter of 1.58 mm, is commonly used for high-quality welding of carbon steels, low-alloy steels, and structural steels, as well as in the fabrication of pressure vessels. The joint preparation followed a double K-groove configuration with four passes: two on each side of the joint. The welding parameters are listed in Table 2.

Table 2 Parameters of the flux cored arc welding process

Parameter	Unit	Value
Current intensity	A	145
Voltage	V	14.3
Beads quantity	–	4
Welding velocity	mm/s	1
Protection gas	–	CO_2
Welding equipment (Miller Model CP-302)	–	–

The welding process parameters were recommended by the steel manufacturer. The FCAW process efficiency is approximately 0.92. Using these values for current intensity, voltage, welding speed, and process efficiency, the added heat was determined to be 2,254 kJ/mm. After the welding process was completed, the welded coupon was allowed to cool in air.

The Charpy impact test is used in this work to determine the fracture toughness K_{Ic} in the welded joint studied. A procedure was designed for this purpose, as shown in Figure 1.

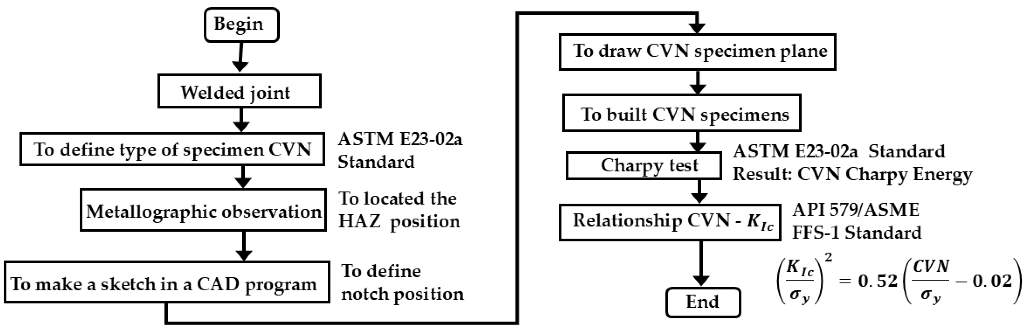

Figure 1 Procedure to determine K_{Ic} in the welded joint

2.1 Integration of Metallography and Computer-Aided Design for Precise HAZ Notch Placement

The procedure begins with the welded joint whose fracture toughness (K_{Ic}) is to be evaluated, followed by the preparation of a Charpy V-notch specimen in accordance with API 579/ASME FFS-1 (American Petroleum Institute (API), 2016) and ASTM E23-02a (10 × 10 × 55 mm, 2 mm notch depth, 0.25 mm root radius) (ASTM International, 2002). This geometry is employed for the experimental and numerical assessment of absorbed energy, and similar configurations have been used for the estimation of fracture toughness and stress analysis around the notch (Kori et al., 2024; Lee et al., 2025). The resulting parameter represents an estimated effective plane strain fracture toughness, derived from empirical correlation, and should not be interpreted as a formally measured ASTM K_{Ic} value obtained through standardized fracture mechanics tests.

A metallographic examination is conducted to accurately locate the heat-affected zone (HAZ), where the notch must be machined. Comparable methodologies have been reported that combine Charpy testing and numerical simulation of welded joints (Yang et al., 2025). The micrograph in Figure 2, in which the filler metal, base metal, and HAZ are clearly distinguished, serves as the geometric reference for notch positioning.

A CAD sketch of the specimen is then created using the nominal dimensions. The 5 mm scale visible in the micrograph is used for calibration by drawing a 5 mm × 5 mm reference square and scaling the inserted image to match this dimension, ensuring dimensional consistency. Subsequently, the remaining geometry is traced, allowing the precise placement of the V-notch within the HAZ. This procedure determined that proper alignment of the notch tip requires machining its center 2 mm from the weld-bead edge (Figure 2). The measured HAZ width was approximately 0.698 mm.

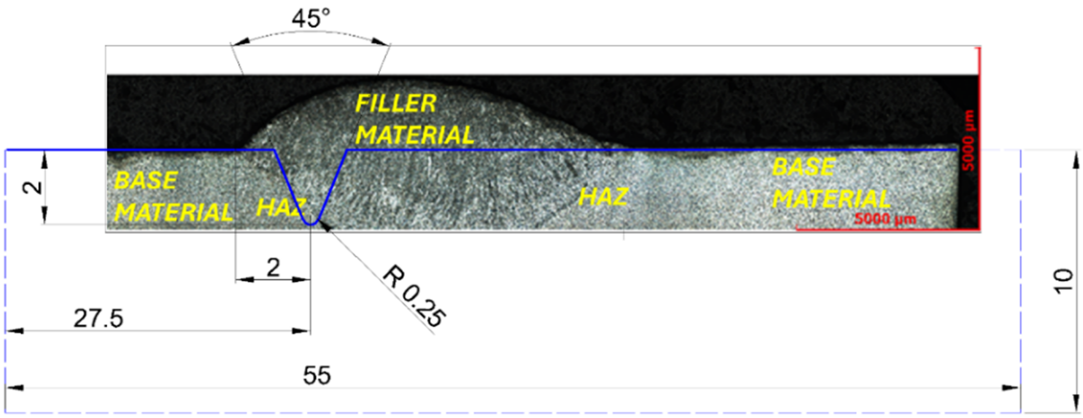

Figure 2 Metallography and diagram to obtain the HAZ position in a CAD system (dimensions in millimeters)

The next step is to fabricate the specimens. A coupon was manufactured from 300 mm × 55 mm and 10 mm thick plates that were welded using FCAW.

Charpy V-notch tests were conducted on a JB-300 pendulum impact machine (Jinan Testing Equipment Co., Ltd., Shandong, China). Tensile properties were measured using an Instron 5982 universal testing machine (Norwood, USA). The pendulum's energy is 150 J. The number of specimens was determined according to the E23-02a standard (ASTM International, 2002).

The last step of the procedure is to determine the fracture toughness based on the energy consumed by the specimen in the Charpy impact test.

2.2 Estimation of the fracture toughness

An average Charpy impact test with V-notch (CVN) energy and the average yield limit were used to estimate the fracture toughness using Equation (1).

$$\left(\frac{K_{Ic}}{\sigma_y}\right)^2 = 0.52\left(\frac{CVN}{\sigma_y} - 0.02\right) \tag{1}$$

To meet the requirements of reproducibility and metrological traceability, the dominant sources of uncertainty associated with the following were recorded: (i) the Charpy CVN absorbed energy measurement, (ii) the tensile yield strength σ_y, and (iii) key geometric dimensions of the specimen (thickness, width, and notch parameters), as well as the notch location within the HAZ. The combined uncertainty of the measurand is evaluated using a mathematical model and the law of uncertainty propagation (GUM approach).

To facilitate uncertainty propagation, Equation (1) is explicitly rewritten as a function of the CVN and σ_y:

$$K_{Ic} = \sigma_y\sqrt{0.52\left(\frac{CVN}{\sigma_y} - 0.02\right)} \tag{2}$$

Since K_{Ic} is an indirect measurand calculated from CVN and σ_y, its combined standard uncertainty is estimated using the law of uncertainty propagation (GUM), assuming independence between CVN and σ_y:

$$u^2\left(K_{Ic}\right) = \left(\frac{\partial K_{Ic}}{\partial CVN}\right)^2 u^2(CVN) + \left(\frac{\partial K_{Ic}}{\partial \sigma_y}\right)^2 u^2\left(\sigma_y\right) \tag{3}$$

From Eq. (2), the sensitivity coefficients are obtained as follows:

$$\frac{\partial K_{Ic}}{\partial CVN} = \frac{0.26}{\sqrt{0.52\left(\frac{CVN}{\sigma_y} - 0.02\right)}} \tag{4}$$

$$\frac{\partial K_{Ic}}{\partial \sigma_y} = \sqrt{0.52\left(\frac{CVN}{\sigma_y} - 0.02\right)} - \frac{0.26\,CVN}{\sigma_y\sqrt{0.52\left(\frac{CVN}{\sigma_y} - 0.02\right)}} \tag{5}$$

The standard input uncertainties were evaluated following the GUM methodology, combining Type A (statistical repeatability) and Type B (instrument calibration and resolution) contributions. Consequently, the combined standard uncertainties of the Charpy V-notch (CVN) energy and the yield limit σ_y were calculated as follows:

$$u(CVN) = \sqrt{\left(\frac{s_{CVN}}{\sqrt{n_{CVN}}}\right)^2 + u_{res,CVN}^2}, \qquad u(\sigma_y) = \sqrt{\left(\frac{s_{\sigma}}{\sqrt{n_{\sigma}}}\right)^2 + u_{cal,\sigma}^2} \tag{6}$$

where s_{CVN} and s_σ are the sample standard deviations;
n_{CVN} and n_σ are the numbers of repetitions;
u_{cal} is the calibration contribution (certificate or equipment traceability);
$u_{res,CVN}$ is the resolution contribution (quantization/reading) of the impact machine, all taken from specifications/certificates.

Table 3 summarizes the instruments used and their technical specifications (range, resolution, and accuracy) according to the manufacturer's data sheets and/or the calibration certificates available for this study to document the minimum metrological support.

Table 3 Instruments, resolution, and reference values for the uncertainty budget

Quantity	Instrument / Method	Typical Resolution / Specification	Distribution Model	Suggested Standard Uncertainty
CVN (J)	JB-300 Charpy pendulum	Energy reading resolution: ±1 J (performance verified under ASTM E23/NIST criteria)	Rectangular + Type A	Type B (resolution): $u_{res,CVN}$; Type A (repeatability): $u_{A,CVN} = \frac{s_{CVN}}{\sqrt{n_{CVN}}}$
σ_y (MPa)	Instron 5982	Load accuracy: ±0.5% of reading (Instron 5900 series)	Rectangular + Type A	Type B (calibration): $u_{cal,\sigma} = \frac{0.005\,\sigma_y}{\sqrt{3}}$; Type A (repeatability): $u_{A,\sigma} = \frac{s_\sigma}{\sqrt{n_\sigma}}$
Specimen dimensions (mm)	Caliper / Micrometer / Calibrated CAD	Tolerance: ±0.02 mm (caliper), ±0.01 mm (micrometer)	Rectangular	$u = \frac{tol}{\sqrt{3}}$ (tol = 0.01 mm)
Notch–HAZ position (mm)	CAD calibrated with 5 mm micrographic scale bar	Global positioning uncertainty: ±0.05 mm (includes scale calibration and HAZ boundary identification)	Rectangular	$u_{HAZ-pos} = \frac{0.05}{\sqrt{3}}$

2.3 Impact load estimation

In this study, an equation was proposed to determine the impact load. The deduction of this equation is as follows:

First, it is necessary to consider some considerations, such as

1. The Charpy specimen functions as a simply supported beam to which a load is applied at the midpoint.
2. At the moment of impact, the two bodies remain united.
3. All the potential energy of the Charpy pendulum is transformed into the potential energy of the deformation, that is, energy losses due to vibrations, friction in the bearings, friction with air, and any other existing energy loss are disregarded. The pendulum manufacturer considers these energy losses during the machine calibration.

To estimate the impact load from the absorbed Charpy energy, the energy-based derivation assumes an elastic energy representation. Consequently, the model does not explicitly capture plastic dissipation, strain rate sensitivity, or detailed dynamic response; rather, it provides an engineering approximation for interpreting the uninstrumented Charpy impact energy within a simplified mechanical framework.

Figure 3 shows the assumed analysis scheme to perform these calculations. To determine the loads acting on the beam, the dynamic load P_{din} is applied, which corresponds to the action of the hammer of the Charpy pendulum on impact. Because the beam is symmetrical, the reactions in the supports are equal and are half of the dynamic load (Figure 3a). Similarly, the Charpy specimen has a notch, indicating that the cross-sectional geometric characteristics vary with the beam length. According to the points in Figure 3b, the geometric characteristics vary as follows:

- Section a–b: does not vary with the height of the cross-section, i.e., it is constant.
- Sections b–c: varies with the cross-section height according to the equation of a line.

- Sections c–d: varies with the height of the cross-section according to the circumference arc equation.

The coordinates (x, y) of a, b, c, and d are (dimensions in millimeters): a(0, 10), b(26.672, 10), c(27.25, 8.25), d(27.5, 8).

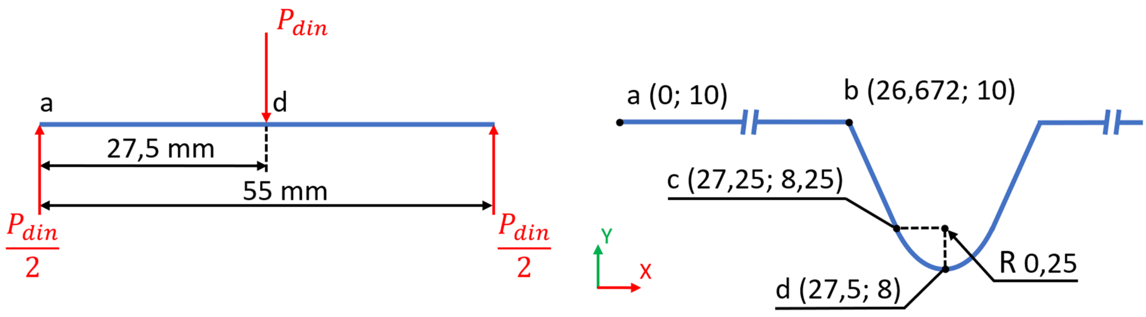

a) b)

Figure 3 Analysis scheme. a) Beam with loads. b) Sections into which the notch is divided to evaluate the variation of the geometric characteristics

The proposed energy model is based on the equivalence between the absorbed energy and the elastic internal strain energy. In elastic bending, the strain energy is expressed as follows:

$$U_d = \int_0^L \frac{M^2(x)}{2EI_x(x)} dx \tag{7}$$

Where $M(x)$ is the bending moment, E is Young's modulus, and $I_x(x)$ is the moment of inertia. According to the work-energy theorem in the idealized scheme, the energy absorbed by the specimen is equal to the external work done by P_{din} at the point of impact:

$$U = W \tag{8}$$

Work at the point of impact is approximated as follows:

$$W = \frac{1}{2} P_{din}\, \delta_{din} \tag{9}$$

Where δ_{din} is the displacement at the midpoint. To relate P_{din} and δ_{din}, Mohr's integral (unit load method) is applied considering a variable section:

$$\delta_{din} = \int_{z_1}^{z_2} \frac{M_k\, M_i}{E\, I_x}\, dz \tag{10}$$

The moment of inertia is evaluated as follows:

$$I_x(z) = \frac{B\, H^3(z)}{12} \tag{11}$$

Where B is the width (10 mm) and $H(z)$ is the effective height. Three sections are considered according to the notch geometry: a–b (constant height), b–c (linear variation), and c–d (circular arc). With the coordinates (in mm) A(0,10), B(26.672,10), C(27.25,8.25), and D(27.5,8), the following equation is used:

For sections b–c:

$$H(z) = -3.03z + 90.816 \text{ [mm]} \tag{12}$$

For sections c–d:

$$H(z) = \sqrt{R^2 - (z - 27.5)^2} + 8.25 \text{ [mm]} \quad \text{with} \quad R = 0.25 \text{ mm} \tag{13}$$

Simpson's composite rule was applied to each subinterval a–b, b–c, and c–d using a uniform mesh in z to evaluate Equation (10) with minimal algebraic complexity. This quadrature results in the following linear proportionality:

$$\delta_{din} = P_{din}\, C_\delta \tag{14}$$

Where C_δ is the geometric coefficient of 4.84×10^{-5}, obtained from the numerical evaluation with $E = 200{,}000$ MPa, $B = 10$ mm, and the defined geometry (consistent units: N, mm, MPa).

Substituting Equation (14) into Equation (9), the work becomes as follows:

$$W = \frac{1}{2} P_{din}^2\, (4.84 \times 10^{-5}) \tag{15}$$

Solving for P_{din}:

$$P_{din} = \sqrt{\frac{2W}{4.84 \times 10^{-5}}} \tag{16}$$

Assuming independence between U and C_δ, the combined standard uncertainty of P_{din} is expressed as follows:

$$u^2(P_{din}) = \left(\frac{\partial P_{din}}{\partial U}\right)^2 u^2(U) + \left(\frac{\partial P_{din}}{\partial C_\delta}\right)^2 u^2(C_\delta) \tag{17}$$

which can be written in relative form as follows:

$$\frac{u(P_{din})}{P_{din}} = \frac{1}{2}\sqrt{\left(\frac{u(U)}{U}\right)^2 + \left(\frac{u(C_\delta)}{C_\delta}\right)^2} \tag{18}$$

In this work, $u(U)$ was obtained directly from the standard uncertainty of the Charpy energy $u(CVN)$, defined in Equation (6), considering the conversion 1 J = 1000 N · mm; therefore:

$$u(U) = 1000\, u(CVN) \tag{19}$$

For its part, $u(C_\delta)$ integrates the contributions associated with the following: (i) uncertainty of the Young's modulus E used in the numerical evaluation, (ii) dimensional tolerances (especially the width B and the geometry associated with $H(z)$), and (iii) numerical quadrature error associated with the Simpson's discretization. The following relative terms were used:

$$\frac{u(C_\delta)}{C_\delta} = \sqrt{\left(\frac{u(E)}{E}\right)^2 + \left(\frac{u(B)}{B}\right)^2 + u_{geom}^2 + u_{num}^2} \tag{20}$$

2.4 Charpy impact test simulation

Figure 4 shows the finite element model developed in SolidWorks Simulation Premium (Dassault Systèmes). Figure 4a shows the Charpy V-notch geometry; Figure 4b defines the boundary conditions and the applied load P_{din}, modeled as static to represent the impact instant; Figure 4c illustrates the quadratic solid elements with localized refinement at the notch tip to capture stress gradients and crack-tip displacements; and Figure 4d indicates the notch-tip location.

Although the Charpy test involves dynamic loading, previous studies have indicated that the effective loading rate can be treated as quasi-static for estimating the fracture parameter (Cao et al., 2020). It is well established that increasing the strain rate reduces apparent toughness due to limited stress relaxation in the plastic zone, which explains why Charpy results typically underestimate toughness compared to CTOD measurements, while better representing impact-dominated behavior (Cao et al., 2020; Lee et al., 2025). A refined mesh was generated considering the 0.25 mm notch radius, and local mesh control was applied at the crack tip. A convergence study was conducted using a static load of 1,000 N, with total displacement and the Stress Intensity Factor at the crack tip as evaluation parameters. Table 4 summarizes the convergence results.

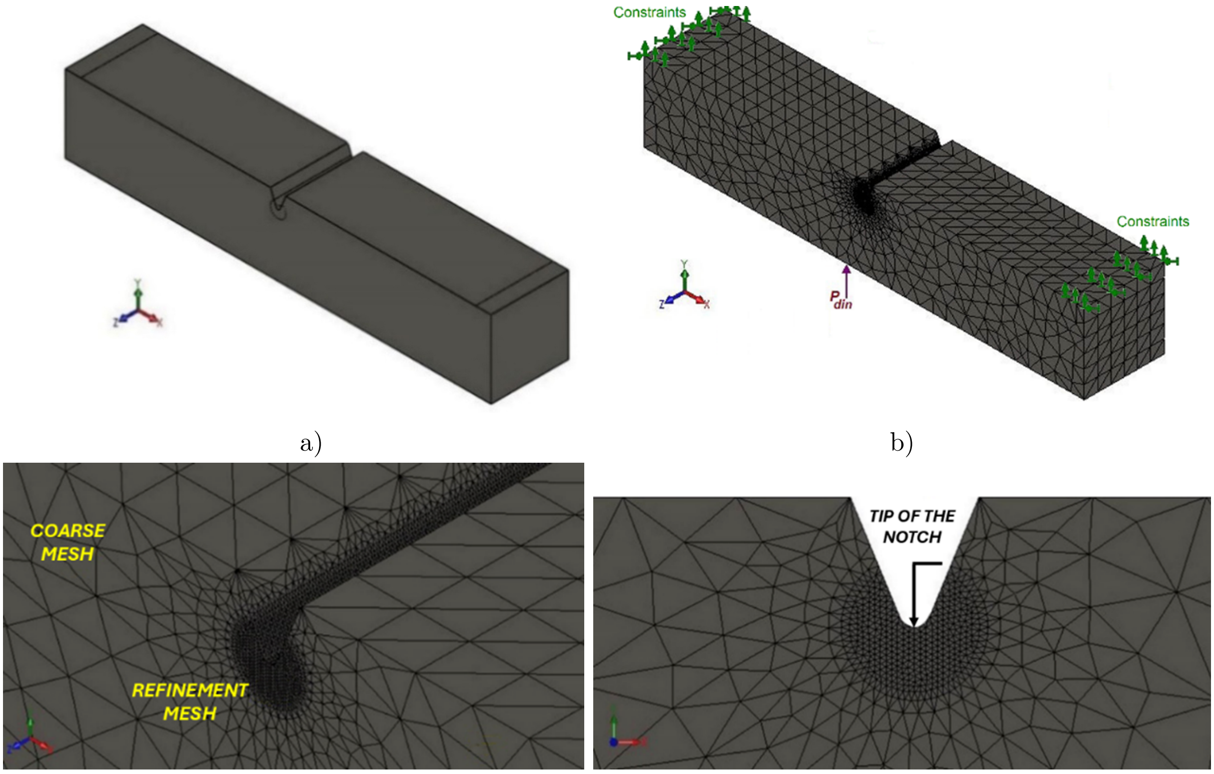

a) b) c) d)

Figure 4 Geometric model, boundary conditions, and finite-element mesh used for Charpy impact simulation

Table 4 Study of mesh convergence around the V-notch tip

Study no.	Finite element size (mm)	Displacement (mm)	Error (%)	Stress Intensity Factor (MPa·m$^{1/2}$)	Error (%)
1	0.125	0.32272	–	2.028	–
2	0.1	0.34465	6.36	4.441	54.34
3	0.09	0.34482	0.05	4.673	4.97

Figures 4b–4d show the final refined mesh around the crack tip. A quadratic tetrahedral solid mesh was used in SolidWorks Simulation to accurately capture strain gradients near the crack front and improve CTOD evaluation, consistent with the superior performance of higher-order elements reported by Dwivedi et al. (2023). The global element size was 1.76341 mm (±0.027 mm), resulting in 91,412 nodes and 61,138 elements, ensuring adequate resolution with reasonable computational cost.

2.4.1 Assumptions regarding the material behavior

In the present finite element model, the material was assumed to be homogeneous, isotropic, and elastoplastic, as defined by the experimentally determined Young's modulus and welded joint's yield strength.

Although welded joints exhibit microstructural heterogeneity among the base metal (BM), heat-affected zone (HAZ), and weld metal (WM), the V-notch was intentionally located within the HAZ based on metallographic characterization. Consequently, the region that controls crack initiation corresponds to the HAZ material. Within the framework of linear elastic fracture mechanics (LEFM), the Stress Intensity Factor K_I depends primarily on the geometry, applied load, and crack size; therefore, a locally homogeneous representation is considered an appropriate first-order approximation (Cao et al., 2020; Kori et al., 2024).

A sensitivity analysis using a three-zone model (BM–HAZ–WM) with ±25% variation in σ_y = 315 MPa showed no change in the crack-tip displacement (0.000444 mm) used in the CTOD-based SIF calculation. These results support the use of a homogeneous material model for Charpy simulation.

3. Results and Discussion

This section presents the experimental and numerical findings that support the proposed procedure for evaluating fracture toughness in the HAZ. The results of the fractographic and microstructural analyses, Charpy impact tests, and finite element simulations (FEM) are examined to validate the accuracy and applicability of the Charpy–Mohr method. Their comparison provides insight into the welded joint behavior under impact loading.

3.1 Fractographic and microstructural analysis of the samples

The hardness test was conducted according to ASTM E18-22 (ASTM International, 2022) using an INCOR TH320 digital durometer with a load of 981 N. The load and reading times were 5 and 2 s, respectively. The hardness of the coarse-grained region of the HAZ was 82 HRB. According to ASTM E112-13 (ASTM International, 2013), using the comparison method, the grain size in the HAZ is number 3, with an average length of 110 μm.

The material's mechanical behavior in the heat-affected zone (HAZ) was interpreted based on the fracture surface analysis of the tested Charpy specimen (Figure 5). The fracture clearly initiates at the notch's root, where the normal stresses reach their maximum value under the impact of the pendulum. From this point, the crack propagates in Mode I from the top of the specimen, as observed in the region identified as the "initial fracture." This behavior confirms that the geometric stress concentrator triggered the fracture criterion and that crack initiation occurred in the region where the notch was intentionally positioned during machining.

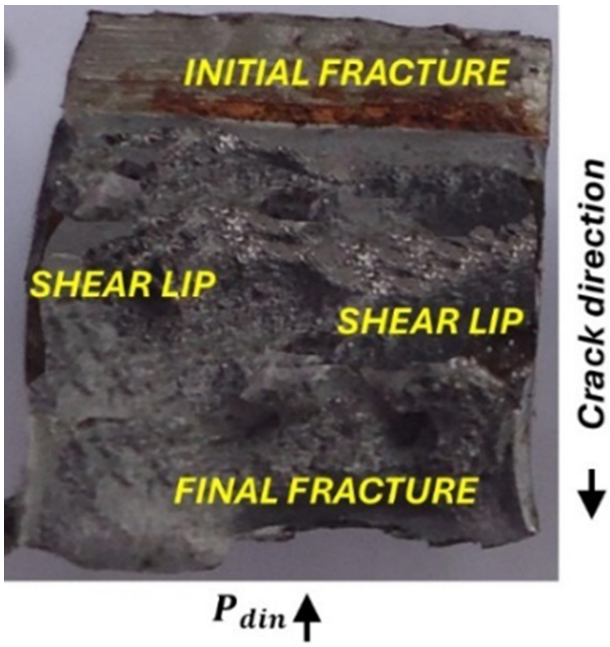

Figure 5 Fracture surface of the Charpy specimen indicating crack initiation, final fracture, and shear lips, together with crack and load directions

The fracture surface exhibits characteristics typical of ferritic–pearlitic steels under impact loading. The central region exhibits a granular, relatively brittle morphology associated with the transgranular fracture of pearlite and limited deformation at high strain rates. In contrast, the lateral edges display asymmetric shear lips linked to ferrite-rich zones that permit greater plastic deformation. This brittle core–ductile edge combination is characteristic of low-carbon steels.

The less defined shear lips compared to the base metal, together with the brittle central zone, are consistent with fracture patterns reported for the HAZ in welded low-alloy steels, where thermal cycles promote grain coarsening, phase heterogeneity, and toughness reduction (Jovanovic et al., 2022; Viseras Pico et al., 2022). Unlike the base metal, which typically exhibits more symmetrical ductile features, or the weld metal, which exhibits solidification-induced heterogeneity, the observed morphology corresponds to the HAZ fracture behavior.

The CAD-assisted notch positioning method is validated by the fact that crack initiation occurred within the metallographically targeted HAZ. Once confirmed, the fracture toughness of the HAZ was quantified using the Charpy–Mohr correlation.

3.2 Calculation of the fracture toughness

The fracture toughness of the welded joint (K_{Ic}) was determined under impact loading using the Charpy impact test. Welded specimens with V-notches (CVN) were fabricated using the FCAW process. The energy required to fracture the specimens was obtained in this experiment (see Table 4).

To calculate the fracture toughness of the welded joint, we considered the yield strength obtained from the tensile test. The yield strength, σ_y, was 315 MPa. Table 5 shows the average absorbed energy from the Charpy V-notch impact tests (CVN) as 29.5 J.

Table 5 Charpy impact test results for FCAW specimens with V-notch AISI 1015 steel and E71T-1 wire

Specimen	CVN (J)
C-FCAW 1	26.0
C-FCAW 2	25.0
C-FCAW 3	38.0
C-FCAW 4	29.0
C-FCAW 5	26.0
C-FCAW 6	40.0
C-FCAW 7	22.5
Average	29.5

The statistical characteristics of the absorbed energy data were evaluated before calculating fracture toughness. Seven Charpy V-notch tests were performed ($n = 7$), yielding a mean absorbed energy of $\overline{U} = 29.5$ J with a standard deviation of $s = 6.79$ J, corresponding to a variation coefficient of 23.0%. The 95% confidence interval of the mean, estimated using Student's t-distribution, ranges from 23.2 J to 35.8 J. No significant outliers were detected according to the Grubbs test ($\alpha = 0.05$). These results suggest that the observed dispersion is consistent with the HAZ's intrinsic variability rather than anomalous measurements.

The fracture toughness correlation presented previously is reformulated here to continue the study:

$$\left(\frac{K_{Ic}}{\sigma_y}\right)^2 = 0.52\left(\frac{CVN}{\sigma_y} - 0.02\right) \tag{21}$$

Using the average experimental values of CVN and σ_y, the fracture toughness in the HAZ was calculated as follows:

$$K_{Ic} = 62.19 \text{ MPa} \cdot \text{m}^{1/2}$$

This value represents the effective resistance to crack propagation in the heat-affected zone under impact loading conditions and is subsequently compared with the stress intensity factor estimated numerically to evaluate failure susceptibility.

Metallurgical Interpretation

As a low-carbon steel, AISI 1015 exhibits fracture toughness that is highly sensitive to microstructural transformations induced by the welding thermal cycle. In the HAZ, grain growth and the localized formation of harder microconstituents generate heterogeneities that reduce the effective ductility and increase the stress concentration at the crack tip.

The obtained value of $K_{Ic} = 62.19$ MPa·m$^{1/2}$ together with an average absorbed energy of 29.5 J, is consistent with the expected behavior of the HAZ in welded structural steels. When compared with the range reported for the base material (41–69 MPa·m$^{1/2}$) (Modulus Metal, 2024), a reduction of approximately 10% is observed. This decrease can be attributed to microstructural transformations, residual tensile stresses, and abrupt property gradients between the base metal and the weld metal. These results confirm that the HAZ represents the critical fracture resistance region, highlighting the relevance of the proposed experimental–numerical procedure for its characterization.

Uncertainty Analysis K_{Ic}

The uncertainty budget of K_{Ic} was constructed following the law of uncertainty propagation described in Equations (3)–(6), considering the experimental inputs (CVN and σ_y) and the metrological characteristics summarized in Table 3. Table 6 presents the input values, their associated standard uncertainties, the sensitivity coefficients derived from Equation (13), and the individual contributions to the combined uncertainty $u(K_{Ic})$.

Table 6 Uncertainty budget for K_{Ic}, obtained from the experimental mean values of CVN and σ_y (Eqs. (2)–(6))

Input quantity	Value	Standard uncertainty	Sensitivity coefficient	Contribution
CVN (J)	29.5	$u(CVN) = 0.54$ J	$\frac{\partial K}{\partial CVN} = 1.34$	0.73
σ_y (MPa)	315	$u(\sigma_y) = 4.7$ MPa	$\frac{\partial K}{\partial \sigma_y} = 0.070$	0.33

Using the correlation of Equation (13), the fracture toughness is calculated as follows:

$$K_{Ic} = 62.19 \text{ MPa} \cdot \text{m}^{1/2}$$

The combined standard uncertainty is:

$$u(K_{Ic}) = 0.79 \text{ MPa} \cdot \text{m}^{1/2}$$

For a coverage factor of $k = 2$, the expanded uncertainty becomes:

$$U(K_{Ic}) \approx 1.6 \text{ MPa} \cdot \text{m}^{1/2}$$

Thus, the fracture toughness can be reported as follows:

$$K_{Ic} = 62.19 \pm 1.6 \text{ MPa} \cdot \text{m}^{1/2}$$

Corresponding to an approximate 95% confidence level.

The uncertainty analysis makes explicit that the dominant contribution arises from the absorbed energy measurement, while the yield strength uncertainty has a smaller influence. This confirms that the impact energy dispersion is the principal driver of uncertainty in the estimation of fracture toughness.

3.3 Calculation of the impact load

Solving for the equivalent dynamic load in the Charpy impact test yields, assuming $U = W$ and using $\overline{U} = 29.5$ J $= 29500$ N $\cdot$ mm, applying Equation (16), we obtain:

$$P_{din} = \sqrt{\frac{2\,(29\,500)}{4.84 \times 10^{-5}}} = 34\,914.3 \text{ N} \tag{4}$$

Uncertainty associated with P_{din}

To apply Equation (20), the following uncertainty components were considered: $u(CVN) = 0.54$ J, $u(E)/E = 0.02$, $u(B)/B = 0.002$, $u_{geom} = 0.01$, and $u_{num} = 0.005$.

From these contributions, the relative standard uncertainty of the geometric factor was obtained as $u(C_\delta)/C_\delta = 0.0230$.

For an absorbed energy $\overline{U} = 29.5$ J and the dynamic load P_{din} calculated from Equation (16), the uncertainty propagation is summarized in Table 7.

Table 7 Uncertainty budget for the equivalent dynamic load P_{din} (Eqs. (17)–(21))

Input	Value	Standard (relative) uncertainty	Factor in $u(P_{din})/P_{din}$	Relative contribution
U (energy)	29.5 J	$\frac{u(U)}{U} = \frac{u(CVN)}{CVN} = \frac{0.54}{29.5} = 0.0183$	$\frac{1}{2}$	0.00915
C_δ (geometric factor)	4.84×10^{-5}	$\frac{u(C_\delta)}{C_\delta} = 0.0230$	$\frac{1}{2}$	0.01150

From Table 7, the combined relative standard uncertainty is as follows:

$$\frac{u(P_{din})}{P_{din}} = \sqrt{(0.00915)^2 + (0.01150)^2} = 0.0147 \tag{22}$$

Thus, the standard uncertainty is:

$$u(P_{din}) = 0.0147 \times 34\,914.3 = 5.1 \times 10^2 \text{ N} \tag{23}$$

For a coverage factor $k = 2$, corresponding to an approximately 95% confidence level, the expanded uncertainty becomes the following:

$$U(P_{din}) = k\,u(P_{din}) = 2\,u(P_{din}) \approx 1.0 \times 10^3 \text{ N} \tag{24}$$

Therefore, the equivalent dynamic load is reported as follows:

$$P_{din} = 34\,914.3 \pm 1.0 \times 10^3 \text{ N}$$

As shown in Table 7, the dominant contribution to the uncertainty of P_{din} comes from the geometric term C_δ, followed by the uncertainty associated with the energy U.

3.4 Fracture toughness estimation by numerical simulation

The Charpy impact test was simulated numerically to estimate the fracture toughness (K_{Ic}) of the welded joint, with an absorbed energy of 29.5 J. Figure 6a illustrates the stress distribution, showing peak von Mises stresses concentrated on the notch, where fracture is initiated, exceeding the material's yield strength.

Figure 6b shows that 76.93% of the specimen volume experiences stresses above yield, indicating extensive plastic deformation. Although significant yielding was observed, the SIF evaluation was performed within a small-scale yielding approximation at the crack tip. This stress concentration near the notch agrees with the findings of Kori et al. (2024).

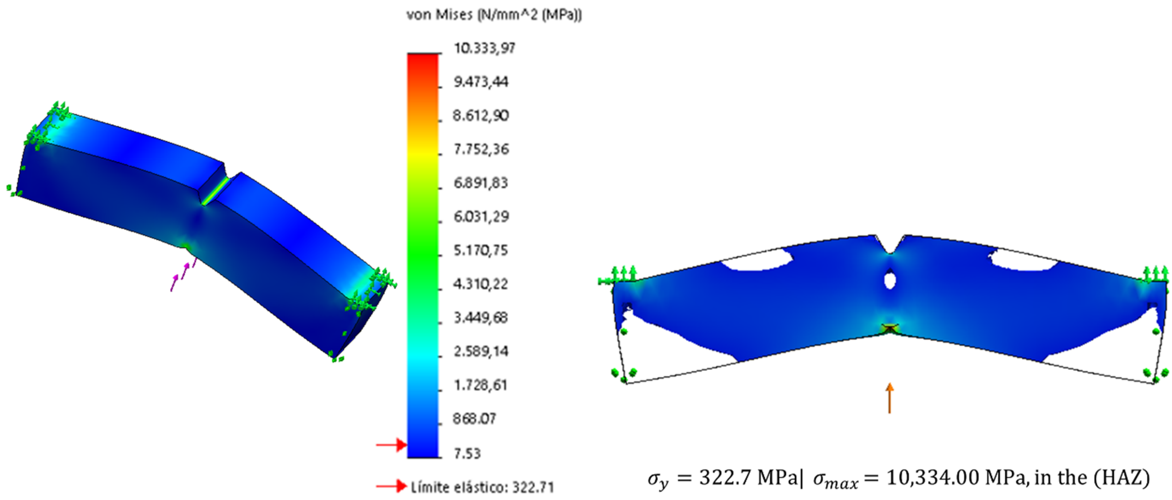

a) b)

Figure 6 Von Mises stress distribution in Charpy simulation: (a) stress field under load; (b) deformed shape with stress contours and yield limit

Figure 7 shows the displacements in the X direction, which were selected because they are normal to the crack plane and determine its opening. Table 8 summarizes the displacements at the crack tip on faces A (front) and B (back) in Figure 7a. These regions correspond to the section transition and the highest stress concentration, where the fracture is expected to initiate.

Table 8 Displacement in the X-direction (U_x) at the crack tip for the front and back faces

Face A: Front surface ($Z = 10$ mm)

Node	Point	U_x (mm)	X (mm)	Y (mm)	Z (mm)
3	V5	-4.033×10^{-3}	27.3611	-1.9579	10.0000
4	V4	-1.999×10^{-3}	27.4274	-1.9892	10.0000
5	V1	-9.10×10^{-5}	27.5000	-2.0000	10.0000
3539	V2	1.829×10^{-3}	27.5726	-1.9892	10.0000
3540	V3	3.855×10^{-3}	27.6389	-1.9579	10.0000

Face B: Back surface ($Z = 0$ mm)

Node	Point	U_x (mm)	X (mm)	Y (mm)	Z (mm)
119	V5	-3.975×10^{-3}	27.3611	-1.9579	0.0000
118	V4	-1.971×10^{-3}	27.4274	-1.9892	0.0000
117	V1	-7.70×10^{-5}	27.5000	-2.0000	0.0000
2151	V2	1.823×10^{-3}	27.5726	-1.9892	0.0000
2152	V3	3.833×10^{-3}	27.6389	-1.9579	0.0000

Negative displacement values indicate movement in the negative X direction. The procedure used to determine the Stress Intensity Factor (K_I) is described below.

3.5 Determination of the stress intensity factor

Alegre and Cuesta (2010) proposed a procedure for determining the Stress Intensity Factor (K_I) from CTOD, which is assumed in this study. For greater consistency, the correlation previously used for the experimental estimation of fracture toughness (originally Equation 1) and now renumbered as Equation (21) is complemented in the numerical analysis by Equation (25):

$$K_I = \frac{E}{8\left(1-\mu^2\right)}\sqrt{\frac{2\pi}{L}}\left[4\left(V_2 - V_4\right) - \left(V_3 - V_5\right)\right] \tag{25}$$

where:

E: is the Young's modulus. Is equal to 200,000 MPa.

L: is the length of the singular elements. The distance between the nodes is shown in Figure 7b and summarized in Table A1.

μ: is the Poisson coefficient, equal to 0.29.

V_i: are the normal displacements to the crack surface. It is determined as the displacement value indicated in Figure 7b and summarized in Table A1.

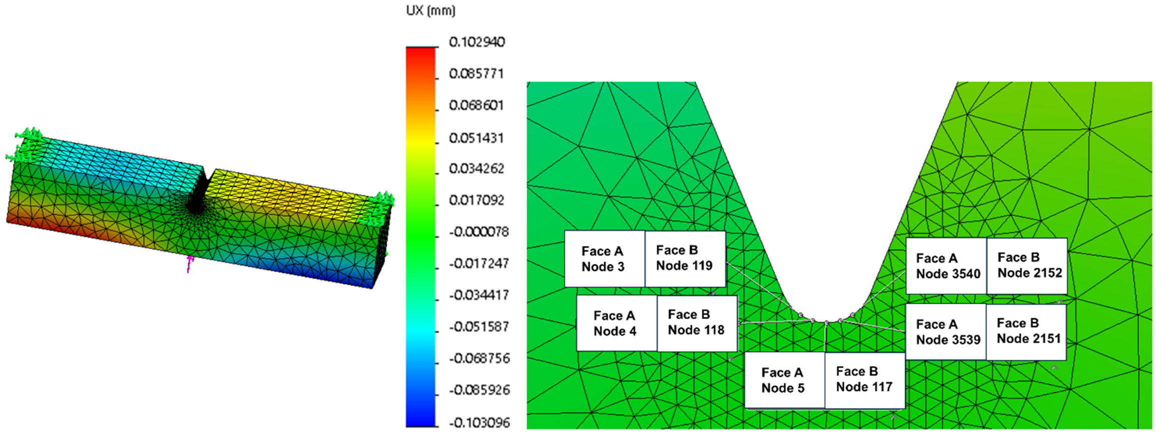

Figure 7 Displacements in the X-axis direction. a) Complete specimen. b) Around the crack tip on the left side

The Stress Intensity Factor (K_I), calculated using Equation 25, was 78.23 MPa·m$^{1/2}$ (22.13%) and 77.64 MPa·m$^{1/2}$ (21.54%) for faces A and B, respectively. The percentages in parentheses indicate the difference relative to the estimated fracture toughness using Equation 13. The discrepancies are attributed to the constitutive material model assumed in this study and the differences between the simulated specimen and the actual test conditions.

According to the fracture mechanics criteria, crack propagation occurs when the following occurs:

$$K_I \leq K_{Ic} \tag{26}$$

Since complete fracture occurred during impact, the applied stress intensity factor approached the critical fracture condition in accordance with the Griffith–Irwin framework. Within the LEFM-based approximation, the numerically computed value (77.94 MPa·m$^{1/2}$) represents the applied stress intensity at failure for the HAZ region, which is obtained as the average of faces A and B.

Charpy-derived fracture toughness (62.19 MPa·m$^{1/2}$) represents an indirect estimate of the material resistance, whereas the FEM value (77.94 MPa·m$^{1/2}$) corresponds to the applied crack-driving force under a pseudo-static assumption. The latter is a numerical consistency check of the energy-based approach rather than an independent measurement of plane-strain toughness. Given the dynamic nature of the Charpy test and the LEFM simplifications, some deviation between both values is expected.

Contextualization of HAZ Fracture Toughness with Respect to Base Material and Structural Steels

The fracture toughness of the HAZ estimated from the Charpy-based correlation was K_{Ic} = 62.19 MPa·m$^{1/2}$, representing a reduction of approximately 10% compared with the upper reference value for AISI 1015 under the as-supply condition (K_{Ic} = 69 MPa·m$^{1/2}$). Although direct ASTM E399 data for AISI 1015 are limited, comparable low-carbon ferritic steels provide useful context. For example, En3B steel reaches values near 90 MPa·m$^{1/2}$ under ductile conditions (Akçay & Oterkus, 2023). Therefore, the obtained HAZ toughness falls within the expected range for this type of steel.

FEM-computed stress intensity factor (K_I = 77.94 MPa·m$^{1/2}$) represents the applied stress intensity under a pseudo-static LEFM approximation and should not be interpreted as a directly measured fracture toughness. The obtained value $K_{Ic} = 62.19$ MPa·m$^{1/2}$ falls within the range of tens to slightly over 100 MPa·m$^{1/2}$, commonly reported for ferritic structural steels tested in the ductile regime (Viseras Pico et al., 2022), supporting the physical consistency of both the experimental and numerical results.

Table 9 compares the current results with those of previous studies on welded joints and HAZ regions, aiming to provide context and order-of-magnitude consistency for the observed values and trends, rather than a one-to-one quantitative comparison. While higher K_{Ic} values are reported for HSLA, bainitic, or duplex steels, the common trend is a marked reduction in toughness in the HAZ. The lower toughness observed in AISI 1015 steel welded using FCAW can be explained by its ferritic-pearlitic microstructure, low carbon content (∼0.15%), and grain thickening induced by the thermal cycling of welding.

The experimental K_{Ic} values were lower than the numerical predictions, which is consistent with the findings reported by Chen et al. (2022) and Singh et al. (2023) for X80 pipe steels. This discrepancy can be attributed to the real microstructural heterogeneities and stress concentrators that are not fully captured in the simulation.

Overall, the agreement between experimental measurements and numerical modeling strengthens the adopted methodology's reliability and the proposed correlations' validity.

4. Conclusions

In this study, an integrated experimental–analytical–numerical procedure was developed for estimating the fracture toughness of the heat-affected zone (HAZ) in FCAW-welded AISI 1015 steel using non-instrumented Charpy impact testing. The metallography–CAD protocol enabled accurate and traceable notch placement within the HAZ, whereas fractographic analysis confirmed that crack initiation occurred at the notch root inside the targeted region. Experimental estimation based on the Charpy–Mohr correlation yielded a fracture toughness of $K_{Ic} = 62.19 \pm 1.6$ ·m$^{1/2}$ ($k = 2$, ≈95% confidence level). The uncertainty analysis showed that the main contribution arises from the dispersion of absorbed impact energy, whereas yield strength uncertainty has a smaller influence. The analytical formulation also allowed the estimation of an equivalent dynamic load of $P_{din} = 34{,}914 \pm 1.0 \times 10^3$ N, establishing a mechanics-based relationship between the absorbed energy and the structural response. The finite element simulation produced a fracture-related value of approximately 77.94 ·m$^{1/2}$, showing reasonable agreement with the experimental estimate. Additionally, an approximate 10% reduction in fracture toughness relative to the base material confirmed that the HAZ is the critical region controlling fracture resistance in the welded joint. Overall, the proposed methodology provides a practical and reproducible alternative for estimating fracture toughness when conventional fracture mechanics testing is not feasible.

Acknowledgements

The authors thank the Center for Innovation and Research in Aeronautical Engineering (CIIIA) of the Autonomous University of Nuevo León for providing the facilities and technical support necessary to carry out the experimental phase of this study. The research stay was funded by Excellence Scholarship Program of the Mexican Ministry of Foreign Affairs.

Author Contributions

Pavel Michel Almaguer Zaldívar: Conceptualization, Methodology, Research, Formal Analysis, Writing – Original Draft; Alexis Cordovés García (*): Conceptualization, Methodology, Visualization, Writing – Review and Editing, Supervision, Project Administration; José Alejandro Martínez Grave de Peralta: Research, Data Curation, Software, Validation; Jesús Rodríguez Flores: Formal Analysis, Data Curation, Writing – Review and Editing; Ricardo Lorenzo Ávila Rondón: Visualization, Validation, Writing – Review and Editing.

Conflict of Interest

The authors declare that there is not conflict of interest.

Supplementary Materials

No supplementary materials were associated with this study.

Declaration of AI

The use of artificial intelligence tools in the preparation of this manuscript was exclusively limited to the editorial process of translating the original text from Spanish into English. For this purpose, ChatGPT (OpenAI) was employed to support the generation of an initial translated version, which was subsequently reviewed and corrected by the authors using Grammarly and through manual revision. All decisions related to the experimental design, data acquisition and analysis, interpretation of the results, and scientific content and final wording are solely the authors' responsibility. The authors assume full responsibility for the accuracy, originality, and integrity of the manuscript.

References

Afzali, N., Jabour, G., Stranghöner, N., & Langenberg, P. (2024a). A comparative study into the fracture toughness properties of duplex stainless steels. *Journal of Constructional Steel Research*, *212*, 108283. https://doi.org/10.1016/j.jcsr.2023.108283

Afzali, N., Jabour, G., Stranghöner, N., & Langenberg, P. (2024b). An investigation into the correlation between fracture toughness and charpy impact test for duplex stainless steels. *International Journal of Offshore and Polar Engineering*, *34*(1), 11–18. https://doi.org/10.17736/ijope.2024.jc926

Ajmal, M., Lopez-Crespo, C., Cruces, A., & Lopez-Crespo, P. (2023). New plastic crack-tip opening displacement tool based on digital image correlation for estimating the fatigue-crack-growth law on 316l stainless steel. *Materials*, *16*(13), 4589. https://doi.org/10.3390/ma16134589

Akçay, F., & Oterkus, E. (2023). Prediction of fracture toughness of metallic materials. *Engineering with Computers*, *39*(1), 81–88. https://doi.org/10.1007/s00366-021-01505-5

Alegre, J., & Cuesta, I. (2010). Some aspects about the crack growth fem simulations under mixed-mode loading. *International Journal of Fatigue*, *32*(7), 1090–1095. https://doi.org/10.1016/j.ijfatigue.2009.12.002

American Petroleum Institute (API). (2016). *Api 579-1/asme ffs-1: Fitness-for-service* (tech. rep.). American Petroleum Institute. Washington, DC, USA.

ASTM International. (2002). *Astm e23-02a: Standard test methods for notched bar impact testing of metallic materials* (tech. rep.). ASTM International. West Conshohocken, PA, USA.

ASTM International. (2013). *Astm e112-13: Standard test methods for determining average grain size* (tech. rep.) (Reapproved 2021). ASTM International. West Conshohocken, PA, USA.

ASTM International. (2020). *Astm e1820-20b: Standard test method for measurement of fracture toughness* (tech. rep.). ASTM International. West Conshohocken, PA, USA.

ASTM International. (2022). *Astm e18-22: Standard test methods for rockwell hardness and rockwell superficial hardness of metallic materials* (tech. rep.). ASTM International. West Conshohocken, PA, USA.

Cao, Y., Zhen, Y., Song, M., Yi, H., Li, F., & Li, X. (2020). Determination of Johnson–Cook parameters and evaluation of charpy impact test performance for X80 pipeline steel. *International Journal of Mechanical Sciences*, *179*, 105627. https://doi.org/10.1016/j.ijmecsci.2020.105627

Chaouadi, R. (2024). Assessing the master curve reference temperature T0 estimated from the charpy impact transition curve and its consequences on the correlation between charpy

DBTT and fracture toughness T0 shifts. *International Journal of Pressure Vessels and Piping*, *208*, 105142. https://doi.org/10.1016/j.ijpvp.2024.105142

Chaouadi, R., Marie, S., Puzzolante, J.-L., Lambrecht, M., Le Gloannec, B., & Cheval, P. (2025). Experimental validation of the charpy-impact based reference temperature T0 of SA 508 heavy forgings of nuclear components and development of a charpy-based fracture toughness lower bound curve. *International Journal of Pressure Vessels and Piping*, *217*, 105544. https://doi.org/10.1016/j.ijpvp.2025.105544

Chen, H., Feng, Q., Bi, Y., Gao, X., Dai, L., & Chi, Q. (2022). Statistical assessment of fracture toughness results from the HAZ of X80 pipeline FCAW girth weld. *Materials*, *15*(17), 6157. https://doi.org/10.3390/ma15176157

de Sonis, E., Dépinoy, S., Giroux, P.-F., Maskrot, H., Wident, P., Hercher, O., Villaret, F., & Gourgues-Lorenzon, A.-F. (2023). Microstructure – toughness relationships in 316l stainless steel produced by laser powder bed fusion. *Materials Science and Engineering: A*, *877*, 145179. https://doi.org/10.1016/j.msea.2023.145179

Dwivedi, K., Pathak, H., & Kumar, S. (2023). Variable node higher-order XFEM for fracture modeling in orthotropic material. *Proceedings of the Institution of Mechanical Engineers, Part C: Journal of Mechanical Engineering Science*, *237*(16), 3692–3716. https://doi.org/10.1177/09544062221148879

El Alami, M., Laazizi, A., & Fri, K. (2024). Numerical analysis EF of resilience impact test behavior for X80 steel. *The International Journal of Advanced Manufacturing Technology*, *131*(7-8), 4107–4128. https://doi.org/10.1007/s00170-024-13258-8

International Organization for Standardization (ISO). (2016). *Iso 148-1:2016. metallic materials — charpy pendulum impact test — part 1: Test method* (tech. rep.). ISO. Geneva, Switzerland.

Jovanovic, M., Camagic, I., Sedmak, S., Sedmak, A., & Burzic, Z. (2022). The effect of material heterogeneity and temperature on impact toughness and fracture resistance of SA 387 Gr. 91 welded joints. *Materials*, *15*, 1854. https://doi.org/10.3390/ma15051854

Kori, T., Kassaye, F., Kozłowska, A., & Grajcar, A. (2024). Numerical modeling of charpy impact toughness behavior and stress distribution of quenching and partitioning steel. *Symmetry*, *17*(1), 53. https://doi.org/10.3390/sym17010053

Kumar, S., Londe, N., Kumar, K., & Kittur, M. (2021). Estimation of fracture toughness (KIC) using charpy impact test for Al6061T6 and Al7075T6 alloys subjected to corrosion. *Materials Today: Proceedings*, *46*(7), 2414–2420. https://doi.org/10.1016/j.matpr.2021.01.298

Lee, J., Jo, W., Seo, J., & An, G. (2025). Effect of notch shape on the fracture toughness behavior. *International Journal of Naval Architecture and Ocean Engineering*, *17*, 100646. https://doi.org/10.1016/j.ijnaoe.2025.100646

Li, H., & Iyama, J. (2024). Investigation on fracture behavior of electroslag welding joint with high-performance steel. *International Journal of Steel Structures*, *24*, 882–891. https://doi.org/10.1007/s13296-024-00855-2

Li, Y., Jiang, T., Li, L., Lu, P., Li, D., Wang, B., Chen, G., & Hou, Y. (2024a). Comparison of destructive and non-destructive fracture toughness measurements for q235 steel butt-welded joint. *Scientific Reports*, *14*, 25218. https://doi.org/10.1038/s41598-024-76687-1

Li, Y., Li, Y., & Chang, J. (2024b). A study on the impact toughness of the simulated heat-affected zone in multi-layer and multi-pass welds of 1000 MPa grade steel for hydroelectric applications. *Metals*, *14*(12), 1455. https://doi.org/10.3390/met14121455

Lojen, G., & Vuherer, T. (2020). Optimization of PWHT of simulated HAZ subzones in P91 steel with respect to hardness and impact toughness. *Metals*, *10*(9), 1–21. https://doi.org/10.3390/met10091215

Modulus Metal. (2024). AISI 1015 annealed carbon steel mechanical properties [Viewed 27 November 2025]. https://www.modulusmetal.com/aisi-1015-annealed-carbon-steel-mechanical-properties/

Narowlansky, Z., Mostafavi, M., Pavier, M., Mokhtarishirazabad, M., & Budden, P. (2024). The effect of welding on brittle fracture: A statistical investigation. *International Journal of Pressure Vessels and Piping*, *208*, 105144. https://doi.org/10.1016/j.ijpvp.2024.105144

Pała, T., & Wciślik, W. (2024). Strength and fracture toughness of TIG- and laser-welded joints of low carbon ferritic steels. *Materials*, *17*, 3956. https://doi.org/10.3390/ma17163956

Pan, J., & Song, C. (2024). Prediction of fracture toughness using small specimens based on machine learning. *Theoretical and Applied Fracture Mechanics*, *132*, 104493. https://doi.org/10.1016/j.tafmec.2024.104493

Peinado, G., Carvalho, C., & Baptista, C. (2024). Effects of interrupted aging T6I4 on hardness and fracture toughness of aeronautic AA7050 alloy. *Journal of the Brazilian Society of Mechanical Sciences and Engineering*, *46*(8), 498. https://doi.org/10.1007/s40430-024-05069-5

Purnama, D., Winarto, W., Sofyan, N., Prihastomo, A., & Ito, K. (2020). Microstructure and mechanical properties of AH-36 steel weldment welded using magnesium modified E6013 electrode. *International Journal of Technology*, *11*(1), 48–59. https://doi.org/10.14716/ijtech.v11i1.2737

Shin, Y.-T., Jung, C.-J., Bae, S.-H., An, G., Son, M., & Park, Y.-I. (2025). Characteristics of microstructure and fracture toughness according to the groove shape of submerged arc welding. *Metals*, *15*(1), 10. https://doi.org/10.3390/met15010010

Singh, M., Arora, K., Gupta, A., Kumar, R., Shukla, D., & Jhunjhunwala, P. (2023). Experimental characterization of dynamic fracture toughness behavior of X80 pipeline steel welded joints for different heat inputs. *Welding in the World*, *67*(3), 617–636. https://doi.org/10.1007/s40194-022-01391-5

Viseras Pico, M., Carnero Moya, M., González Palma, R., & Muñoz Rubio, A. (2022). Analysis of the fracture toughness in the heat affected zone (HAZ) of one HSLA steel. *DYNA*, *97*(5), 543–548. https://doi.org/10.6036/10506

Yang, Q., Wang, Y., Li, D., Liu, R., Wang, C., & Zhao, J. (2025). Research on charpy impact test and simulation of laser welded joints in 6252 armor steel. *Theoretical and Applied Fracture Mechanics*, *138*, 104920. https://doi.org/10.1016/j.tafmec.2025.104920

Yildiz, R. (2022). Evaluation of fracture toughness and charpy V-notch test correlations for selected Al alloys. *European Mechanical Science*, *6*(1), 1–8. https://doi.org/10.26701/ems.913428